FTIR spectroscopy of OH stretching modes in BSO, BGO and BTO sillenites



1994 J. Phys.: Condens. Matter 6 6329

(http://iopscience.iop.org/0953-8984/6/31/032)

J. Phys.: Condens. Matter 6 (1994) 6329–6344. Printed in the UK

# FTIR spectroscopy of OH stretching modes in BSO, BGO and BTO sillenites

P Beneventi†, R Capelletti†, L Kovács‡, Á Péter‡, A M Lanfredi Manotti§ and F Ugozzoli§

† Department of Physics, University of Parma, Viale delle Scienze, 43100 Parma, Italy and Consorzio Interuniversitario Nazionale di Fisica della Materia

‡ Research Laboratory for Crystal Physics, Hungarian Academy of Sciences, 1112 Budapest, Budaörsi út 45, Hungary

§ Institute of General and Inorganic Chemistry, University of Parma, Viale delle Scienze, 43100 Parma, Italy

Received 17 March 1994

**Abstract.** High-resolution (0.05 $cm^{-1}$) FTIR spectroscopy in the temperature range 9–320 K has been used to monitor the narrow line absorption spectra, induced by the stretching modes of OH and OD impurities in as-grown and in-deuterated samples of BSO, BGO, mixed $(1-x)$BSO·$x$BGO, and BTO sillenite single crystals (i.e. $Bi_{12}MeO_{20}$ with Me=Si, Ge and Ti). The model of the anharmonic oscillator in the Morse potential was applied to interpret the observed spectra and the anharmonicity parameter $x_e$ determined. For the line peaking at 3442.84 $cm^{-1}$ in BSO both the fundamental and the first overtone transitions were detected: in this way the complete set of the Morse parameters could be determined. A model for the OH centre is proposed on the basis of the dependence of the line position against lattice constant in all the systems examined. The phonon coupling of the stretching modes observed was studied by analysing the detailed temperature dependence of the line position and width. In the framework of weak coupling theory the frequencies of coupled phonons were determined and found to be in agreement with those obtained by reflectance, Raman scattering measurements and theoretical calculations.

## 1. Introduction

Sillenite is a BCC structure associated by Sillen [1] to the $\gamma$-phase of $Bi_2O_3$. Compounds of $Bi_2O_3$ with small amounts of a large list of metal oxides ($MeO_2$) crystallize in such a structure and are described by the the general formula $Bi_{12}MeO_{20}$. BSO, BGO, and BTO (with Me=Si, Ge and Ti) are among such compounds.

The sillenite symmetry corresponds to the I23 space group [2]. The Me atom is surrounded by four oxygen atoms ($O_{(3)}$) located at the corners of a tetrahedron; such tetrahedra are at the corners and at the centre of the unit cubic cell. Three Bi atoms are located at equal distances of each $O_{(3)}$; each Bi atom is surrounded by seven oxygens: among them the $O_{(2)}$ is located on the principal diagonal of the unit cell, one is an $O_{(3)}$, and the other five are indicated as $O_{(1)}$ [2]. X-ray diffraction measurements [2] suggest that BGO crystals grow in non-stoichiometric composition: i.e. ~9% of Bi excess is present.

BSO, BGO, and BTO are large gap semiconductors (the optical energy gap $E_g$ being in the range 3.1–3.4 eV). A shoulder overlaps the onset of the absorption edge in undoped samples [3] and can be suppressed by doping with a proper impurity (for example Al, Fe,

0953-8984/94/316329+16$19.50  

Ga and P) [4,5]. An antisite $Bi^{3+}$ ($Bi_{Me}$), i.e. a bismuth ion, located at the $Me^{4+}$ site and charge-compensated by a hole, is assumed to be responsible for the shoulder [4,6].

These materials exhibit many interesting properties, such as strong rotatory power, piezoelectricity, photorefractive effect, electric field induced linear and circular birefringence, which make such materials attractive for advanced technological applications [7].

Defects induced by the presence of impurities (for example transition metals, rare earths) in sillenites have been extensively investigated, by using a variety of spectroscopies [7]. However very little has been reported [8,9], at least to our knowledge, about defects such as OH, which are common in many insulating crystals as alkali halides or oxides [10–15]. Since sillenite single crystals are grown in air, OH is expected to enter the crystal. Moreover hydrogen impurities are good candidates for the thermal fixing of the holographic gratings, as in the case of $LiNbO_3$ [8,16]: therefore it is worthwhile to study the properties of defects induced by the possible presence of OH-impurities in sillenites.

OH can be detected by monitoring the stretching mode absorption band in the infrared range. Therefore high-resolution (0.05 $cm^{-1}$) FTIR absorption spectra have been measured in the temperature range 9–320 K for as grown (in the wavenumber ranges 3400–3600 and 6400–7000 $cm^{-1}$) and for deuterated samples (in the wavenumber range 2500–2600 $cm^{-1}$) of BSO, BGO, BTO, and mixed BSO–BGO. The model of the anharmonic oscillator in the Morse potential [17] was applied to interpret the observed spectra. The dependence of the main stretching frequency against the sillenite lattice constants was investigated in order to propose a model for the defect responsible for the main band. The phonon coupling of stretching modes was studied by analysing the temperature dependence of the line position and half-width.

## 2. Experimental details

The reagent powders used to grow BSO, BGO, and BTO were $Bi_2O_3$ and $GeO_2$ prepared in the Research Laboratory for Crystals Physics (Budapest) from 5N pure metal rods by chemical digestion, while $SiO_2$ and $TiO_2$ were Johnson Matthey grade A1 oxides.

BSO, BGO and mixed BSO–BGO crystals were grown by the balance controlled Czochralski technique, in air, using resistance heating and a platinum crucible. The boules were pulled along the [001] direction at the rate of 0.7 mm $h^{-1}$ and rotation speed of 15 $min^{-1}$. The diameter and length of the crystals were 21 mm and 40–50 mm, respectively. The melts were prepared from the pre-calcined mixture (740 °C, 24 h) of oxide compounds of nominal composition $(1-x)$BSO·$x$BGO with $x = 0$, $x = 0.25$, $x = 0.5$, $x = 0.75$ and $x = 1$. However, it should be stressed that the actual BGO molar fraction in the crystal may be different from the nominal one, as can be concluded from lattice constant measurements (see figure 7). Mixed BSO–BGO crystals were grown on BGO seeds.

The incongruently melting BTO crystals were grown from solution by the top seeding technique. The melt was prepared from the mixture of $Bi_2O_3$ and $TiO_2$ compounds in the molar ratio of 8:1. Before seeding, the melt was homogenized for 24 h at 950 °C. The crystals were pulled on BGO seeds, along the [001] direction at the rate of 0.3 mm $h^{-1}$ and with the rotation speed of 6 $min^{-1}$. During the growth run the furnace was cooled at the rate of 0.4 °C $h^{-1}$.

Oriented samples were cut from each crystal and the (100) planes were polished. The size of the samples used was $10\times10\times11.8$ $mm^3$ for the thick samples and $10\times10\times1.2$ $mm^3$ for the thin ones.

The high-resolution optical absorption measurements were performed by means of a

Bomem DA8 FTIR spectrophotometer operating in the range 7000–200 $cm^{-1}$, with an apodized resolution as good as 0.04 $cm^{-1}$. The absorption spectra were measured in the temperature range 9–320 K, by assembling the sample in a 21SC model Cryodine Cryocooler of CTI-Cryogenics.

The infrared (IR) spectroscopy measurements were performed both on 'as grown' (i.e. not submitted to any treatment after the crystal growth and the sample preparation) and on deuterated samples. The isotopic substitution of H with D was obtained by heating the samples at $\sim$ 800 °C in dry $O_2$ flowing through $D_2O$.

Single crystal x-ray measurements by means of a Philips PW1100 four circle diffractometer using Mo-$K_\alpha$ radiation ($\lambda$=0.7107 Å) were carried out at room temperature (RT) to obtain accurate cell parameters for each compound.

The cell parameters were obtained by a least-squares fit of

$$(1/d)^2 = h^2a^{*2} + k^2b^{*2} + l^2c^{*2} + 2hka^*b^*\cos\gamma^* + 2klb^*c^*\cos\alpha^* + 2hlc^*a^*\cos\beta^* \quad (1)$$

where $d$ is the spacing between planes of Miller indices $hkl$ and the starred variables are the reciprocal lattice parameters. A least-squares fit of equation (1) with the restriction of the cubic crystal system led to the $d$ values reported in table 2. The value of $d$ for any family of planes of Miller indices $hkl$ were introduced in the calculation after accurate measurements of sets of reflections: $\pm h, 0, 0$; $0, \pm k, 0$; $0, 0, \pm l$; $\pm h, \pm h, 0$; $0, \pm k, \pm k$; $h, h, h$ and some other intense reflections. Each reflection was repeatedly centred until the Bragg angle shift was not more than 0.01°. Then the antireflection was also measured to remove any error in the instrumental zero.

The standard deviations were calculated according to the propagation of error law. The crystalline samples showed high mosaicity, in agreement with the high values of the estimated standard deviations (see table 2).

## 3. Results

Typical high-resolution absorption spectra measured at 9 K on 'as grown' samples of BSO, BGO and BTO in the range 3420–3520 $cm^{-1}$ are shown in figure 1.

A few lines are present in BGO and BTO and usually only one in BSO (a few very weak lines were observed in thick samples): their position $\Delta G_{10}^{H}$ and the half-maximum full width $W_{10}^{H}$ are summarized in table 1. It should be noted that the lines are very narrow at 9 K, in fact their widths are in the range 0.15–1.34 $cm^{-1}$ and could be resolved only by using the high-resolution FTIR spectroscopy. A line peaking at 3445 $cm^{-1}$ at RT has been already reported in BSO, BGO, and BTO and attributed to the presence of OH [9]: however its width has been found to be as large as 10–20 $cm^{-1}$. This value is considerably larger than those found in the present work (6.05 $cm^{-1}$ for BSO, 5.5 $cm^{-1}$ for BGO and 5.98 $cm^{-1}$ for BTO at RT).

The spectra are heavily affected by the temperature at which they are measured: in fact the lines shift to lower wavenumbers, broaden and weaken by increasing the temperature, as shown by figure 2 in the case of a BGO sample. The lines peaking at 3438.87, 3480.99 and 3498.36 $cm^{-1}$ at 9 K can no longer be detected at temperatures higher than 150 K (see figure 2), while the main line, peaking at 3450.85 $cm^{-1}$, is still present, even if broad and weak, at higher temperatures, at least up to 320 K (not shown in figure 2 for the sake of clarity).

The detailed analysis of the line position against temperature, stresses that the 3442.84 $cm^{-1}$, 3450.85 $cm^{-1}$ and 3456.60 $cm^{-1}$ lines in BSO, BGO and BTO respectively, show nearly the same temperature shift, as shown in figure 3. This characteristic behaviour suggests that

**Table 1.** Parameters related to the OH and OD absorption lines measured at 9 K in BSO, BGO and BTO. $\Delta G_{10}^{H}$ is the line position in the as-grown crystal; $W_{10}^{H}$ is the related half maximum width; $\Delta G_{10}^{D}$ is the line position in the deuterated sample; $W_{10}^{D}$ is the related half maximum width; $x_e$ is the anharmonicity parameter, as evaluated from equation (11), by assuming $\rho = 0.5300$ related to the free diatomic molecule.

| Matrix | $\Delta G_{10}^{H}$ ($cm^{-1}$) | $W_{10}^{H}$ ($cm^{-1}$) | $\Delta G_{10}^{D}$ ($cm^{-1}$) | $W_{10}^{D}$ ($cm^{-1}$) | $x_e$ ($\times 10^2$) |
|---|---|---|---|---|---|
| BSO | 3442.84 [a] | 0.44 | 2545.53 | 0.24 | 2.712 |
| | 3447.45 [b] | | | | |
| | 3448.58 [b] | | | | |
| | 3449.86 | 0.27 | | | |
| BGO | 3438.87 | 1.45 | | | |
| | 3450.85 [a] | 0.25 | 2551.01 | 0.15 | 2.680 |
| | 3480.99 | 0.23 | 2573.45 | 0.10 | 2.690 |
| | 3498.36 | 0.33 | 2579.13 | 0.25 | 2.223 |
| BTO | 3456.60 [a] | 1.28 | 2555.02 | 0.76 | 2.664 |
| | 3485.56 | 0.95 | | | |
| | 3502.37 | 0.95 | | | |

[a] 'Main band'.

[b] Very weak line, detected only in thick samples.

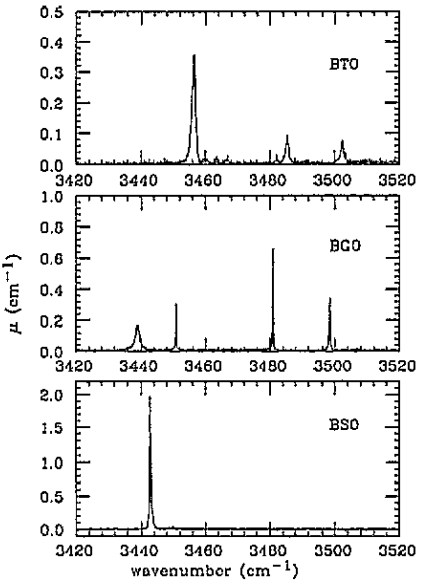


**Figure 1.** High-resolution (0.05 $cm^{-1}$) optical absorption spectra of BSO, BGO and BTO sillenites measured at 9 K in the range 3420–3520 $cm^{-1}$.

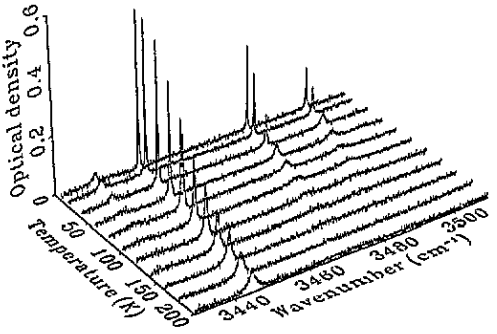


**Figure 2.** High-resolution (0.05 $cm^{-1}$) optical absorption spectra of BGO measured at different temperatures. Spectra in the range 3430–3520 $cm^{-1}$: at 9 K, 20 K, 40 K, 60 K, 80 K, 100 K, 120 K, 140 K, 160 K, 180 K and 200 K.

particular attention should be given to the above lines: in the following each of them will be indicated as the main line in BSO, BGO and BTO respectively. The temperature dependence of the additional lines, e.g. those mentioned in the above paragraph, reveal remarkably

different behaviour, as can be seen from the normalized position $\Delta G^{H}_{10}(T)/\Delta G^{H}_{10}(9\ K)$ (i.e. ratio of the wavenumber at which the maximum occurs at a given temperature $T$ to that at 9 K) of the lines against temperature.

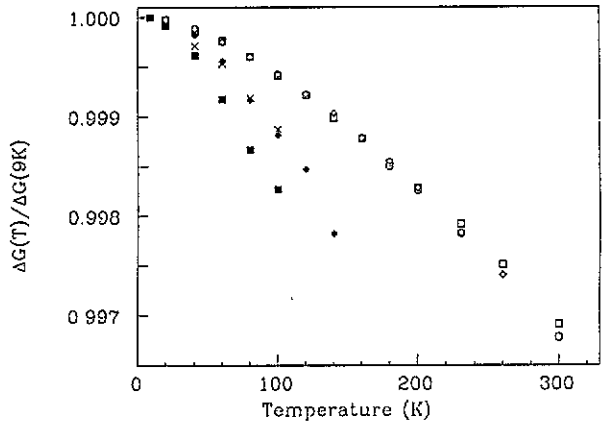


**Figure 3.** Normalized line position against temperature for the main lines in BSO (open diamonds), BGO (open circles) and BTO (open squares) and for the additional lines in BGO: line at 3438.87 $cm^{-1}$ (crosses), at 3480.99 $cm^{-1}$ (full diamonds) and at 3498.36 $cm^{-1}$ (full squares). The normalized position $\Delta G^{H}_{10}(T)/\Delta G^{H}_{10}(9\ K)$ is the ratio of the wavenumber at which the maximum occurs at a given temperature $T$ to that at 9 K.

In order to support the hypothesis that the lines, or some of the lines, shown in figure 1 are due to hydrogen-related defects in sillenite crystals, the spectra of deuterated samples (see section 2) were measured at 9 K in the range 2500–2600 $cm^{-1}$, see figure 4. In fact, as a consequence of the isotopic substitution of H with D, a shift of the spectrum towards the lower wavenumbers is expected since the oscillator frequency ($\Delta G^{H}_{10}$ or $\Delta G^{D}_{10}$) is inversely proportional to the square root of the defect reduced mass ($\mu_H$ or $\mu_D$), according to

$$\frac{\Delta G^{H}_{10}}{\Delta G^{D}_{10}} \sim \sqrt{\frac{\mu_D}{\mu_H}}. \tag{2}$$

The expected shift occurs indeed for the main line in BSO, BGO and BTO, as shown in figure 4. The isotopic replicas of the stronger additional lines have also been detected. The position and the width of the observed lines are collected in table 1.

Due to the 0.2 % natural abundance of $O^{18}$ isotope, lower wavenumber satellite lines are expected to appear beside the bands assumed to belong to OH defects. Indeed, a very weak line at 3432.09 $cm^{-1}$ has also been observed in a $\sim$ 4 cm thick BSO sample at 9 K. Its wavenumber corresponds to that of the isotopic replica of the main line assuming the validity of equation (2) by substituting H and D with $O^{16}$ and $O^{18}$, respectively. The satellite line intensity roughly agrees with that calculated from the natural abundance of $O^{18}$, however, an unambiguous assignment can only be obtained after the isotopic exchange of the oxygens in the crystal.

The H–D shift expected on the basis of equation (2) is verified within 2–3%: anharmonicity effects could account for the difference [17]. On this basis we analysed the wavenumber region 6400–7000 $cm^{-1}$ where first overtone transitions might occur for the defects responsible for the lines appearing in the 3400–3600 $cm^{-1}$ range (fundamental transitions). In a very thick sample ($\sim$ 4 cm) of BSO a very weak line was detected peaking at 6701.94 $cm^{-1}$ at 9 K, see figure 5: it can be associated to the first overtone transition for the defect responsible for the main line at 3442.84 $cm^{-1}$.

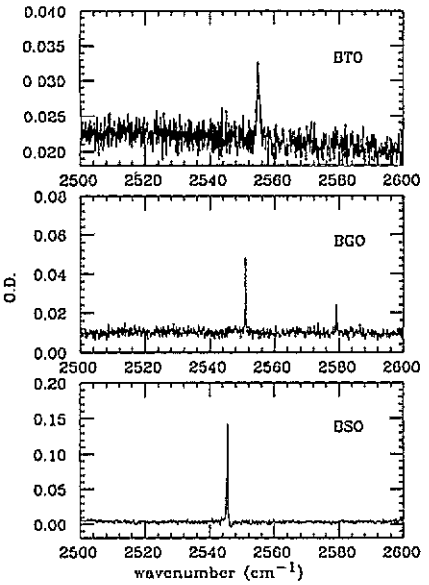


**Figure 4.** High resolution (0.05 cm$^{-1}$) optical absorption spectra of deuterated BSO, BGO and BTO sillenites measured at 9 K in the range 2500–2600 cm$^{-1}$.

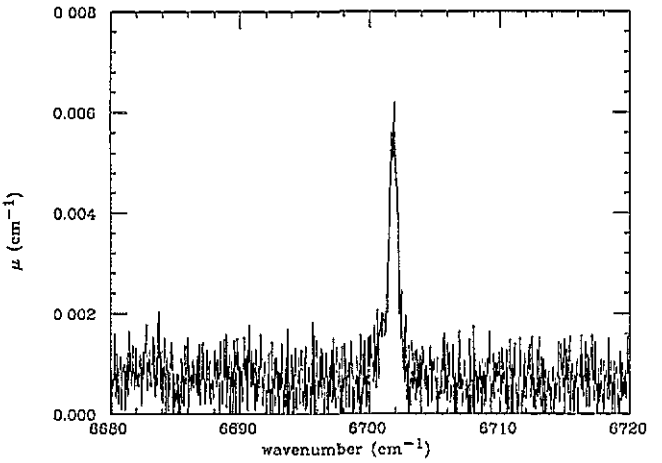


**Figure 5.** High-resolution (0.05 cm$^{-1}$) optical absorption spectra of a thick (~ 4 cm) BSO sample measured at 9 K in the range 6680-6720 cm$^{-1}$.

The absorption spectra of mixed crystals $(1-x)$BSO·$x$BGO were also measured at 9 K in the region 3420–3520 cm$^{-1}$: they are displayed in figure 6 together with the spectra of the extreme compositions (i.e. BSO: $x = 0$ and BGO: $x = 1$), for the sake of comparison. It turns out that the main band shifts gradually from the position in pure BSO to that in pure BGO by increasing $x$, moreover, it remarkably broadens or splits. The addition of BGO to BSO causes the appearance of the other lines detected in the pure BGO. Again they shift and broaden in the mixed crystals. The position and the width of the observed lines are collected in table 2 together with the lattice constants measured.

**Table 2.** Lattice constants $d$ measured at RT, line position $\Delta G_{10}^{H}$ and related half maximum width $W_{10}^{H}$, measured at 9 K, in $(1-x)$BSO·$x$BGO mixed systems and in BTO. In the last column the OH concentration $c_{OH}$, estimated from the main band according to equation (12), at 300 K is shown.

| $x$ fraction | $d$(Å) | $\Delta G_{10}^{H}$ (cm$^{-1}$) | $W_{10}^{H}$ (cm$^{-1}$) | $c_{OH} \times 10^{-15}$ |
|---|---|---|---|---|
| 0.00 | 10.09404 ± 0.00846 | 3442.84 [a] | 0.44 | 37–40 |
| 0.25 | 10.12188 ± 0.00462 | 3434.41 | ~7 | |
| | | 3447.66 [a] | 2.74 | 10 |
| | | 3478.14 | 2.36 | |
| | | 3495.93 | 2.11 | |
| 0.50 | 10.10840 ± 0.01202 | 3446.44 [a] | 2.85 | 34 |
| | | 3477.13 | ~2.45 | |
| | | 3495.25 | ~2.1 | |
| 0.75 | 10.12483 ± 0.01110 | 3434.57 | ~2 | |
| | | 3438.51 | ~2 | |
| | | 3449.14 [a] | 2.07 [b] | 16 |
| | | 3450.11 [a] | | |
| | | 3479.91 | 1.6 | |
| | | 3497.44 | 1.52 | |
| 1.00 | 10.13281 ± 0.00799 | 3438.87 | 1.45 | |
| | | 3450.85 [a] | 0.25 | 2.1–8.1 |
| | | 3480.99 | 0.23 | |
| | | 3498.36 | 0.33 | |
| BTO | 10.16539 ± 0.00863 | 3456.60 [a] | 1.28 | 16–19 |
| | | 3485.56 | 0.95 | |
| | | 3502.37 | 0.95 | |

[a] 'Main band'.

[b] The width is related to the two overlapping lines, whose position is indicated in the third column.

## 4. Discussion

### *4.1. Attribution of the observed spectra to the presence of OH impurities*

According to the experimental results, the spectra in the range 3420–3520 cm$^{-1}$ show a few lines in BGO and BTO and usually only one in BSO. We attribute the above spectra to the presence of OH in the sample for the following reasons:

(i) The crystals are grown in air, therefore the water molecules present in the atmosphere dissociate at the crystal growth temperature into OH and H: the OH can easily enter the sample, in analogy to what happens in other materials (e.g., alkali halides [10], or oxides as, for example, $SiO_2$ [11], $TiO_2$ [12], $LiNbO_3$ [13, 14] and $Bi_4Ge_3O_{12}$ [15]).

(ii) The observed spectrum appears in the region of the OH stretching mode absorptions reported for other oxides. It should be noted that a line peaking at 3428 cm$^{-1}$ at RT in BSO [8] and a line peaking at 3445 cm$^{-1}$ at RT in BSO, BGO and BTO [9] have already been attributed to the presence of OH.

(iii) As a consequence of the isotopic substitution of H with D, a shift of the spectrum towards shorter wavenumbers is observed (see figure 4), according to (2) where the reduced masses of free OH and OD diatomic molecules are assumed for $\mu_H$ and $\mu_D$ respectively. Similarly, a shift due to $O^{18}$ with respect to $O^{16}$ is also detected.

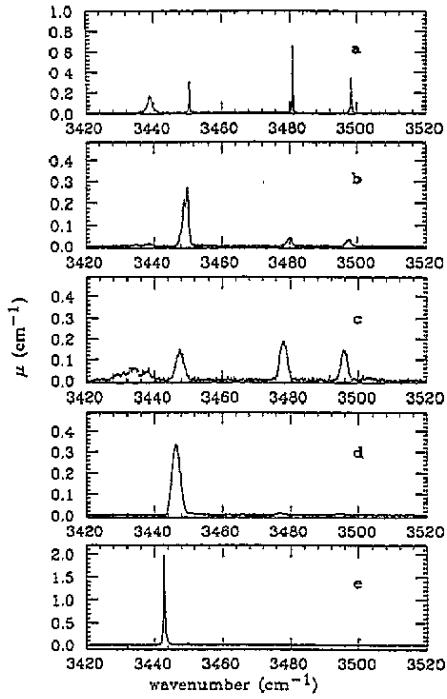


**Figure 6.** High-resolution optical absorption spectra of mixed $(1-x)$BSO·$x$BGO crystals measured at 9 K in the range 3420–3520 $cm^{-1}$. (a) $x = 1$; (b) $x = 0.75$; (c) $x = 0.25$; (d) $x = 0.5$; (e) $x = 0$. The resolution is 0.05 $cm^{-1}$ for $x = 0$ and $x = 1$ (unmixed crystals) and 0.1 $cm^{-1}$ for the other $x$ values.

### *4.2. OH-centres as anharmonic oscillators in the Morse potential*

Equation (2) is fulfilled by the data reported in table 1 for each band within 2–3%. This suggests that anharmonicity effects are expected to occur as for the OH stretching modes in other matrices [17, 10]: therefore the model of the anharmonic oscillator in the Morse potential [17] is applied to analyse the stretching modes, responsible for the absorption spectra of sillenites displayed in figures 1 and 5 (as grown samples) and figure 4 (deuterated samples).

The OH stretching mode transitions can be described in the framework of the anharmonic oscillator in the Morse [17] potential $U$, as a function of the distance $r$:

$$U(r - r_e) = D_e\{1 - \exp[-\beta(r - r_e)]\}^2 \tag{3}$$

where $D_e$ and $\beta$ are the potential parameters ($D_e$ is the binding energy), $r_e$ is the equilibrium distance.

The exact solution of the Schrödinger equation yields the term values $G(n)$ given by

$$G(n) = \omega_e(n + 1/2)[1 - x_e(n + 1/2)] \tag{4}$$

where

$$\omega_e = \beta\left(\frac{\hbar D_e}{\pi c \mu}\right)^{1/2} \tag{5}$$

$$\omega_e x_e = \frac{\hbar \beta^2}{4\pi c \mu} \tag{6}$$

and $\mu$ is the reduced mass of the diatomic molecule. Note that in the above equations $\omega_e$ and $D_e$ are expressed in wavenumbers.

In the case of the anharmonic oscillator the transitions for $\Delta n \neq 1$ are allowed in addition to those for $\Delta n = 1$, at variance with the harmonic oscillator. The wavenumber for the transition $0 \rightarrow n$ is:

$$\Delta G_{n0} = G(n) - G(0) = n\omega_e[1 - x_e(n+1)]. \tag{7}$$

From (7) one can derive $\Delta G_{10}$, $\Delta G_{20}$ (for the $0 \rightarrow 1$ fundamental and the $0 \rightarrow 2$ first overtone transitions, respectively), $x_e$ and $\omega_e$ parameters:

$$x_e = \frac{1}{2}\frac{\Delta G_{20} - 2\Delta G_{10}}{\Delta G_{20} - 3\Delta G_{10}} \tag{8}$$

$$\omega_e = 3\Delta G_{10} - \Delta G_{20}. \tag{9}$$

Therefore measurements of both the fundamental and first overtone transitions allow the determination of $x_e$, $\omega_e$, $\beta$ and $D_e$. The last two are obtained from (5) and (6).

In the case of the main band in BSO it was possible to detect both the fundamental and the first overtone transitions (see section 3 and figures 1 and 5). The parameters evaluated in this way are $x_e = 0.02532$, $\omega_e = 3.62646 \times 10^3$ cm$^{-1}$, $\beta = 2.2726 \times 10^8$ cm$^{-1}$ and $D_e = 35803.1$ cm$^{-1}$ (or 4.417 eV) at 9 K. The value of $x_e$ is comparable with that found, by using the same model, for the stretching mode of free OH molecule (0.0227) [18], for OH stretching modes in $LiNbO_3$ (0.02354, 0.02388, 0.02561) [17], in alkali halides [10] and for OH stretching modes perturbed by Mg-related defects in NaF and LiF [19]. The value of $D_e = 4.417$ eV found in the present case for the binding energy is comparable with those quoted in the literature for free OH and $OH^-$ molecules (4.39 and 4.752 eV respectively) [18] and for OH in $LiNbO_3$ (4.84, 4.81 and 4.45 eV) [17], but lower than that found for OH in alkali halides (from 4.92 for CsI to 5.47 eV for NaF) [20] and for OH perturbed by Mg-related defects in NaF and LiF (5.25 and 5.13 eV) [19].

If hydrogen is substituted by deuterium the reduced mass $\mu$ changes and, as a consequence $\omega_e$, $x_e$ and $\Delta G_{n0}$ change. For example, by defining $\rho$ the ratio between the reduced masses for the OH system to that of the OD system, and $R$ the ratio between the wavenumber of the fundamental transition for the hydrogenated defect $\Delta G_{10}^{H}$ to that of the deuterated defect $\Delta G_{10}^{D}$, i.e.

$$\rho = \frac{\mu_H}{\mu_D} \qquad \text{and} \qquad R = \frac{\Delta G_{10}^{H}}{\Delta G_{10}^{D}} \tag{10}$$

one obtains the anharmonicity parameter $x_e$ as a function of $\rho$ and $R$:

$$x_e = \tfrac{1}{2}(1 - \rho^{1/2}R)(1 - \rho R)^{-1}. \tag{11}$$

Substituting $x_e$, as determined from (8), in (11) one is able to obtain $\rho$: in the case of BSO, where the overtone transition was detected, one obtains $\rho = 0.5313$ from the experimental data. Such a value can be compared, for example, to that of the free diatomic molecule ($\rho_f = 0.5300$), or to that of the oxygen strongly coupled to the lattice ($\rho_c = 0.5364$) [17]. It turns out that the $\rho$ value, experimentally determined, lies between the values of the two oversimplified models, being closer to the value of the free diatomic molecule as in the case of alkali halides and of $LiNbO_3$ [10, 17]. If the overtone transitions are too weak to be detected, as in the case of our BGO and BTO samples, but the fundamental transitions in deuterated samples can be measured (see section 3 and figure 4), $x_e$ can be evaluated by exploiting equation (11). By assuming for $\rho$ the value related to the free diatomic molecule, i.e. $\rho_f$, one obtains $x_e$ values in the range $2\text{–}3 \times 10^{-2}$, for each band whose isotopic replica

can be detected as well. These values, reported in table 1, are in agreement with the $x_e$ values quoted in the literature for the OH stretching modes in oxides and alkali halides [17,20] and obtained by following the same procedure. The values of $x_e$ found for the 'main band' in BSO, BGO and BTO are very close one to the other. In the case of the main band in BSO, $x_e$ can be evaluated by using either (8) or (11). The two values (0.02532 and 0.02712) are different, as expected, since by applying (11) one has to make an assumption on the value of $\rho$: in the present case that of the free diatomic molecule, which turns out to be only an approximation, as shown above.

The anharmonicity parameter can be evaluated by means of a third approach, in fact the ratio of the transition probability for the first overtone to that for the fundamental ($I_{0\to2}/I_{0\to1}$) is found to be $\sim x_e$ in the framework of the Morse oscillator model [17]. From an experimental point of view such a ratio can be evaluated as the ratio of the area under the overtone absorption line to that under the fundamental one. The value of $x_e$ obtained in such a way for the main line transition in BSO is $\sim 3.23 \times 10^{-3}$, i.e. rather different from the $x_e$ value obtained from (8) by using the positions of the fundamental and overtone transitions. This suggests that electrical anharmonicity effects occur in addition to the mechanical ones, i.e. the electrical dipole moment associated to the transition is no longer a linear function of the distance between the two partners of the absorbing molecule [17]. Large electrical anharmonicity effects have been recently reported for OH stretching modes in alkali halides [10].

The above results supply a further support to the attribution of the observed IR spectra of sillenites to the OH stretching modes.

### *4.3. Dependence of $\Delta G^H_{10}$ on the lattice constant*

Wedding and Klein [21] and more recently Lüty and coworkers [10] found that the wavenumber of the OH stretching mode absorption in alkali halides depends on the lattice constant of the host matrix: in particular it decreases by increasing the lattice constant $d$. On this basis we searched for a dependence of the 'main band' position against the lattice constant in sillenites, since figure 1 shows that the 'main band' position changes slightly by changing the host matrix. Therefore lattice constants were measured by means of x-ray diffraction (see section 2) on the same samples of BSO, BGO, BTO and mixed BSO–BGO single crystals on which the absorption spectra were monitored in the region of the OH stretching mode transition (see figures 1 and 6). The values of the measured lattice constant $d$ for each system is reported in table 2: they are slightly different from those quoted in the literature [7] probably due to the high mosaicity of our samples, see section 2. The position $\Delta G^H_{10}$ of the main band in each sample is reported against the lattice constant $d$ (see figure 7). The results show that in sillenites the OH stretching line (main line) wavenumber increases by increasing the lattice constant, at variance with the trend observed in alkali halides.

The discrepancy can be explained by considering that in a simple lattice, such as that of alkali halides, the lattice constant is closely related to the size of the anion which OH is substituting for, as shown by figure 8(a) where $\Delta G^H_{10}$ is plotted against the anion radius [10]. Such a relationship does not necessarily hold for a more complex structure, as that of sillenites with 66 atoms per cubic unit cell [2]. Since it is very likely that OH will occupy an oxygen site, one has to correlate the OH stretching line wavenumber to a nearest-neighbour distance of an oxygen inside the complex structure, rather than to the lattice constant. The distance between oxygens in different sites (see section 1) and bismuth or metal (Me=Si, Ge and Ti) are known from crystallographic studies for BSO, BGO and BTO [2, 22, 23]. For

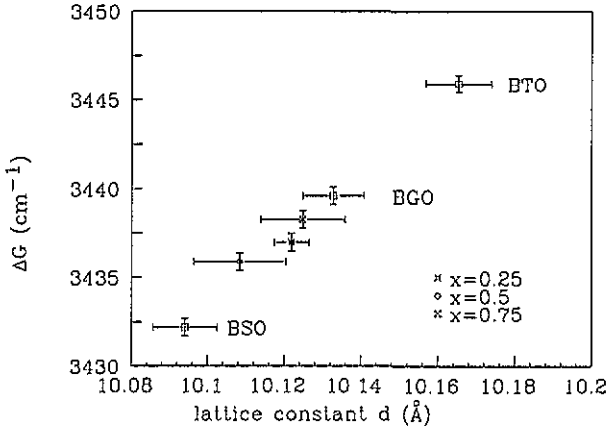


**Figure 7.** Plot of the position $\Delta G_{10}^{H}$ (measured at RT) of the main band in BSO, BGO, BTO and in mixed $(1-x)$BSO·$x$BGO crystals against the lattice constant $d$ measured at RT.

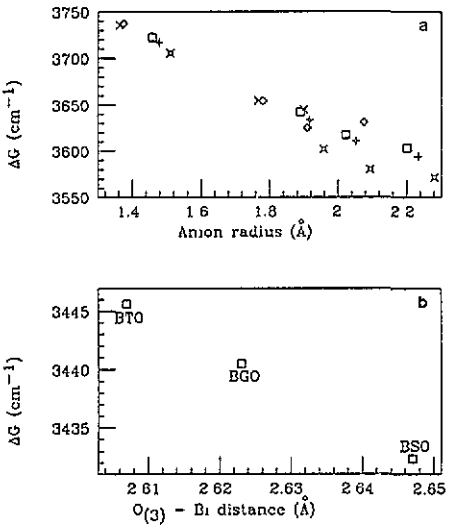


**Figure 8.** (a) Plot of the OH-stretching lineposition $\Delta G_{10}^{H}$ (measured at 15 K) in alkali halides against the anion radius [10]. (b) Plot of the OH-stretching line (main band) position $\Delta G_{10}^{H}$ (measured at RT) in BSO, BGO, BTO against the nearest-neighbour distance $O_{(3)}$–Bi [23].

instance, a plot of the OH stretching line wavenumber against the nearest-neighbour distance $O_{(3)}$–Bi [23] shows a trend similar to that of alkali halides (see figure 8(b)).

The above considerations suggest a possible location and model for the OH defect responsible for the main line in sillenites. The $OH^-$ might substitute an $O_{(3)}$ sitting near an antisite tetrahedrally coordinated $Bi_{Me}^{3+}$ [4, 5]. In this way the negative charge excess introduced by $Bi^{3+}$ is locally compensated by the positive charge excess introduced by $OH^-$ : i.e. $OH^-$ can play the same charge compensation role played by a hole with regard to $Bi^{3+}$ ions present in excess with respect to the stoichiometric composition.

### *4.4. Additional lines*

As shown by figures 1 and 6, in addition to the main line, other absorption lines are detected in BGO and BTO. Some very weak lines are also observed in thick BSO samples.

The relative amplitude of the various lines in BGO (and BTO) depends on the ingot from which the sample has been cut, compare for instance the central curve of figure 1 with the curve at 9 K of figure 2. This result rules out that such lines are due to different transitions between energy levels of the same defect. Some of these lines show their isotopic replica when deuterium is substituted for hydrogen, see figure 4 and table 1. Therefore they should be associated with defects in which hydrogen is involved: they might be tentatively attributed to complexes formed by OH and unwanted impurities already present in the reagent powders, mainly in $GeO_2$.

### *4.5. Evaluation of OH concentration in the samples*

The evaluation of OH concentration from the optical absorption coefficient of the OH stretching mode fundamental transition in the infrared region is usually carried out on the basis of a calibration curve: namely the OH concentration is determined by a proper physical or chemical analysis of a sample on which the IR OH absorption coefficient has been previously measured. Such an approach has been applied to OH in alkali halides [24, 25] and in oxides [26, 27]. Due to the lack of a direct evaluation of the OH concentration in sillenites and in order to get a rough estimate of the OH content responsible for the main band, we used the simple formula

$$c_{OH} = \frac{\mathcal{A}_{int}}{\ln 10\, f} \tag{12}$$

where $c_{OH}$ is the number of OH molecules or ions $cm^{-3}$, $\mathcal{A}_{int}$ is the area under the OH absorption band (expressed in $cm^{-2}$) and $f$ is the so called absorption strength per ion. The $f$ values, determined from proper calibration curves, are available for various materials. By assuming $\mathcal{A}_{int}$ as the area under the main band (measured at 300 K) and $f \sim 9.1 \times 10^{-18}$ cm, evaluated by Klauer *et al* [27] for OH in $LiNbO_3$, a rough estimate of $c_{OH}$ was obtained for each sample by using (12): the results are reported in table 2. Different values of $c_{OH}$ for a given system, displayed in table 2, are related to samples taken from different ingots. Very good reproducibility of $c_{OH}$ in thick and thin samples taken from the same part of the ingot has been observed. It is worthwhile noticing that the $c_{OH}$ values reported in table 2 are reduced roughly by a factor three if $f \sim 2.75 \times 10^{-17}$ cm (instead of $f \sim 9.1 \times 10^{-18}$ cm) is used in (12) according to the Paterson's procedure [26] applied to $SiO_2$ related materials. Such an approach has been followed by Khomich *et al* [9] to determine the OH content in their BSO–BGO mixed samples: the value found by them, by considering the IR absorption band, is in the range $1–3 \times 10^{16}$ $cm^{-3}$ in good agreement with our findings for BSO ($1.2–1.3 \times 10^{16}$ $cm^{-3}$). An OH content of $\sim 2 \times 10^{17}$ $cm^{-3}$ has been reported for BSO by Arizmendi [8].

### *4.6. Phonon coupling*

The phonon coupling of the OH vibrational modes can be studied by analysing the temperature dependence of lineposition and of linewidth.

Since the width of the observed lines is very narrow, one can expect a rather weak phonon coupling of the defect responsible for them to the lattice. A single phonon coupling model is assumed as in the case of the stretching vibrations of H on Si surfaces [28].

In the framework of such an approach, the stretching mode is coupled to a single phonon band, of frequency $\omega_0$ and width $\gamma$, by a coupling constant $\delta\omega$ and allowed to be $|\delta\omega| \ll \gamma$ (weak coupling limit).

Under this assumption the stretching line has a Lorentzian shape and is peaking at $\Delta G(T)$, which is shifted from the zero-temperature position $\Delta G_0$, according to:

$$\Delta G(T) = \Delta G_0 + \delta\omega\left[\exp\left(\frac{hc\omega_0}{kT}\right) - 1\right]^{-1} \tag{13}$$

where $k$ is the Boltzman constant and $h$ is the Planck constant.

The line half-maximum width $W(T)$ is given by:

$$W(T) = W_0 + \frac{2(\delta\omega)^2}{\gamma}\exp\left(\frac{hc\omega_0}{kT}\right)\left[\exp\left(\frac{hc\omega_0}{kT}\right) - 1\right]^{-2} \tag{14}$$

where $W_0$ is the line half-maximum width at $T = 0$ K. Note that in equations (13) and (14) $\omega_0$, $\delta\omega$ and $\gamma$ are expressed in wavenumbers.

In agreement with the above hypothesis, the main lineshape in BSO, BGO and BTO is found to be a Lorentzian, as shown for the sake of example in the case of BGO at 9 K, in figure 9. This means that one is dealing with a homogeneous broadening [29]. More generally the lineshape should be described by a Voigt profile, i.e. by a convolution between a Lorentzian and a Gaussian [30]. In the present case the lineshape analysis in the range 9–300 K, shows that the Lorentzian fraction is close to one, even at temperatures as high as 300 K in BSO and BGO, while decreases from 0.9 to ~ 0.75 in BTO. The lower Lorentzian fraction in BTO can be attributed to the lower crystalline quality.

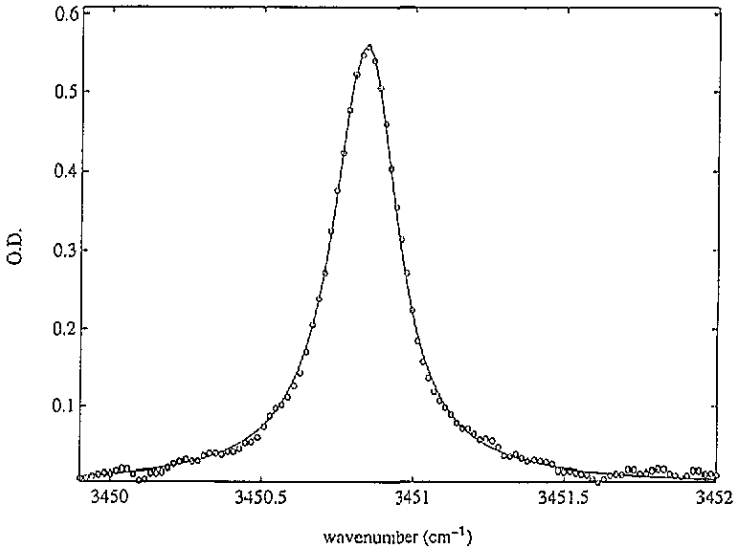


**Figure 9.** High-resolution optical absorption spectrum related to the main line peaking at 3450.85 cm$^{-1}$ in BGO, measured at 9 K: the full line is the result of a fitting of the experimental data (symbols) according to a Lorentzian. The fitting according to the Voigt profile gives a Lorentzian fraction as high as 0.9997. The linewidth is 0.26 cm$^{-1}$.

The position and the width of the lines against temperature fit well to equations (13) and (14), see figure 10, where the position $\Delta G_{10}^{H}$ (on the top) and the width $W_{10}^{H}$ (on the bottom) are plotted against the temperature for a BGO sample. The parameters, such as $\delta\omega$,

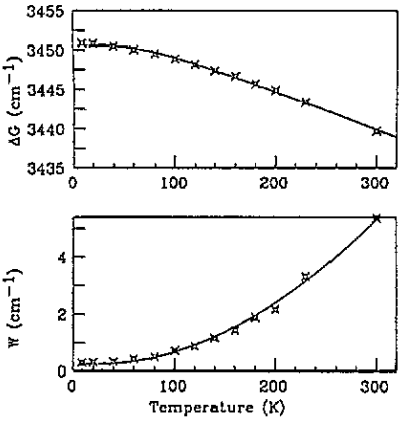


**Figure 10.** Plot of the position $\Delta G_{10}^{H}$ (on the top) and the width $W_{10}^{H}$ (on the bottom) of the main line (peaking at 3450.85 $cm^{-1}$ at 9 K) against temperature for the same BGO sample of figure 9. The full lines show the fitting of the experimental data according to (13) and (14) respectively. The fitting parameters are collected in table 3.

**Table 3.** Phonon coupling parameters as obtained from the fitting to equations (13) and (14) of the lineposition and linewidth against temperature for the main band in BSO, BGO and BTO. $\Delta G_{10}^{H}$ is the lineposition at 9 K, $\delta\omega$ is the coupling constant, $\gamma$ the phonon band width and $\omega_0$ the phonon frequency. For the sake of comparison the lattice frequency $\omega_{IR}$ obtained from IR reflectance measurements [31], $\omega_R$ from Raman scattering measurements [32] and $\omega_{calc}$ from calculations [33] are displayed.

| Matrix | $\Delta G_{10}^{H}$ ($cm^{-1}$) | $\delta\omega$ ($cm^{-1}$) | $\gamma$ ($cm^{-1}$) | $\omega_0$ ($cm^{-1}$) | $\omega_{IR}$ ($cm^{-1}$) | $\omega_R$ ($cm^{-1}$) | $\omega_{calc}$ ($cm^{-1}$) |
|---|---|---|---|---|---|---|---|
| BSO | 3442.84 | 8.99 | 84.03 | 129.83 | 136 | 135.5 | 131.8<br>136 |
| BGO | 3450.85 | 9.66 | 86.02 | 134.42 | 130 | 131.2 | 130.2<br>131.2 |
| BTO | 3456.60 | 8.12 | 80.37 | 121.84 | | 128 | |

$\gamma$ and $\omega_0$, obtained from the fitting of the position and width of the main line in different sillenites, according to (13) and (14), are collected in table 3.

The frequencies of the coupled phonons $\omega_0$, evaluated in this way, are in good agreement with those determined by means of IR reflectance [31] and Raman [32] measurements and with those obtained from theoretical calculations [33], as shown in table 3.

The initial hypothesis $|\delta\omega| \ll \gamma$ turns out to be satisfactorily fulfilled. Therefore the present model of weak coupling between the localized OH stretching mode and the lattice vibrations describes rather well the broadening and the shift of the main line in sillenites. The weak coupling can also account for the very narrow linewidths observed (see table 1).

In the case of mixed $(1-x)$BSO-$x$BGO crystals, all lines are much broader, as shown in figure 6 and in table 2, than those detected in unmixed ones (i.e. for $x = 0$ and $x = 1$). Moreover for $x = 0.75$ the main line splits into two components: however none of them coincides with the lines in the unmixed crystals. Inhomogeneous broadening can be responsible for the remarkable increase of linewidth in mixed crystals. In fact let us assume, according to the model proposed above for the defect responsible for the main

line, that OH substitutes one of the four oxygens at the corners of the tetrahedron located at the centre of the cubic unit cell: for $x \neq 0$ the eight silicon atoms at the corners of the cube are partly substituted by germanium ones. The random distribution of these last and the fact that OH can occupy different corners of the tetrahedron at the centre of the cubic cell may be responsible for many different environments seen by the OH centre. The hypothesis of an inhomogeneous broadening is also supported by the lineshape in mixed crystals: it is no longer a Lorentzian as in the case of unmixed crystals but is described by a Voigt profile [30], even at low temperatures (9 K). In this case the Gaussian contribution, which describes the inhomogeneous broadening, is as high as 60%.

## 5. Conclusions

The above results show that the narrow absorption lines, detected in the 3400–3600 $cm^{-1}$ range in BSO, BGO, mixed $(1-x)$BSO·$x$BGO and BTO sillenite single crystals grown in air, are due to the stretching modes of OH-related defects.

In all the systems examined a line indicated as the 'main line' has a similar temperature dependence in the 9–300 K range. For the defect, responsible for this line, a model has been proposed: an $OH^-$ substitutes an $O_{(3)}$ sitting near an antisite tetrahedrally coordinated $Bi^{3+}_{Me}$. The additional lines are assumed to be caused by complexes of OH and impurity-related defects.

The model of the anharmonic oscillator in the Morse potential has been applied to analyse the fundamental transitions responsible for many lines in as-grown and deuterated samples of BSO, BGO, and BTO and the first overtone of the main line in BSO. The anharmonicity parameters $x_e$ for different OH-related defects and the OH binding energy (obtained only for the defect responsible for the main line in BSO) have been found to be in agreement with those quoted in the literature for OH defects in other oxides and alkali halides.

The detailed analysis of the position and width of the main line against temperature on the basis of a single-phonon coupling model has shown that the OH-stretching mode is weakly coupled to the lattice vibrations. The frequency of the coupled phonon has been determined and found to be in agreement with those obtained from IR reflectance and Raman measurements and from theoretical calculations.

## 6. Acknowledgments

The authors would like to thank Professor Fritz Lüty of The University of Utah at Salt Lake City for having kindly supplied the data related to the OH- and OD-stretching mode positions in alkali halides, widely used for comparison in the present work.

One of the authors (LK) undertook this work with the support of the ICTP Programme for Training and Research in Italian Laboratories, Trieste, Italy. Financial support from the National Science Fund of Hungary (OTKA T4420) and from the Italian 'Consorzio Interuniversitario Nazionale di Fisica della Materia' are acknowledged.

## References

[1] Sillen G 1937 *Ark. Kemi. Mineral. Geol.* **12A** 1
[2] Abrahams S C, Jamieson P B and Bernstein J L 1967 *J. Chem. Phys.* **47** 4034
[3] Hou S L and Aldrich R E 1973 *J. Appl. Phys.* **44** 2652
[4] Oberschmid R 1985 *Phys. Status Solidi* a **89** 263

[5] Grabmaier B C and Oberschmid R 1986 *Phys. Status Solidi* a **96** 199
[6] Reyher H J, Hellwig U and Thiemann O 1993 *Phys. Rev.* B **47** 5638
[7] Arizmendi L, Cabrera J M and Agulló-López F 1992 *Int. J. Optoelectron.* **7** 149
[8] Arizmendi L 1989 *J. Appl. Phys.* **65** 423
[9] Khomich A V, Kargin Yu F, Perov P I and Skorikov V M 1990 *Izv. Akad. Nauk SSSR Neorg. Mater.* **26** 1914
[10] Afanasiev Ch P, An C P and Lüty F 1993 *Proc. Int. Conf. on Defects in Insulating Materials vol 2 (Nordkirchen, 1992)* (Singapore: World Scientific) 551
[11] Krefft G B 1975 *Radiat. Effect.* **26** 249
[12] Bates J B and Perkins R A 1977 *Phys. Rev.* B **16** 3713
[13] Förster A, Kapphan S and Wöhlecke M 1987 *Phys. Status Solidi* b **143** 755
[14] Kovács L, Földvári I, Cravero I, Polgár K and Capelletti R 1988 *Phys. Lett.* 433
[15] Kovács L and Capelletti R 1993 *Proc. Int. Conf. Defects Insulating Materials (Nordkirchen, August 1992)* (Singapore: World Scientific) **2** 1194
[16] Vormann H, Weber G, Kapphan S and Krätzig E 1981 *Solid State Commun.* **40** 543
[17] Fowler W B, Capelletti R and Colombi E 1991 *Phys. Rev.* B **44** 2961
[18] Radzig A A and Smirnov B M 1985 1993 *Reference Data on Atoms, Molecules, and Ions (Springer Series in Chemical Physics)* (Berlin: Springer) pp 381 402
[19] Capelletti R, Beneventi P, Colombi E and Fowler W B *Nuovo Cimento* D **15** 415–28
[20] Afanasiev Ch P, An C P and Lüty F Private communication
[21] Wedding B and Klein M V 1969 *Phys. Rev.* **177** 1274
[22] Zaretskii Yu G, Ukhanov Yu I and Shmartsev Yu V 1991 *Sov. Phys.– Solid State* **33** 681
[23] Zaretskii Yu G, Ukhanov Yu I and Shmartsev Yu V 1991 *Sov. Phys.– Solid State* **33** 685
[24] Fritz B, Lüty F and Anger J 1963 *Z. Phys.* **174** 240
[25] Guckelsberger K 1980 *J. Phys. Chem. Solids* **41** 1209
[26] Paterson M S 1982 *Bull. Mineral.* **105** 20
[27] Klauer S, Wöhlecke M and Kapphan S 1992 *Phys. Rev.* B **45** 2786
[28] Dumas P, Chabal Y J and Higashi G S 1990 *Phys. Rev. Lett.* **65** 1124
[29] Svelto O 1989 *Principles of Lasers* (New York: Plenum) p 30
[30] Di Bartolo B 1968 *Optical Interactions in Solids* (New York: Wiley) p 357
[31] Wojdowski W, Lukasiewicz T, Nazarewicz W and Żmija J 1979 *Phys. Status Solidi* b **94** 649
[32] Venugopalan S and Ramdas A K 1972 *Phys. Rev.* B **5** 4065
[33] Wojdowski W 1985 *Phys. Status Solidi* b **130** 121